

# The fluid dynamics of an underfloor air distribution system

By Q. A. LIU AND P. F. LINDEN

Department of Mechanical and Aerospace Engineering, Jacobs School of Engineering,  
University of California, San Diego, 9500 Gilman Drive, La Jolla, CA 92093-0411, U.S.A.,

(Received 30 May 2005)

This paper discusses the fluid dynamics of an under floor air distribution (UFAD) ventilation system. In order to produce more realistic models of UFAD systems, we extend previous work on a simplified system consisting of a single heat source at floor level and a single cooling diffuser developed by Lin & Linden (2005), to the case of multiple cooling diffusers and a single heat source located at different heights above the floor. We carry out experiments in which the heat source is represented as a buoyant plume, and the cooling diffusers are modelled using negatively buoyant vertical jets. The experiments show that the properties of the system are determined by the entrainment into the plumes and the negatively buoyant jets. In the spirit of Morton, Taylor & Turner (1956), we characterize these entrainment processes by entrainment coefficients, and develop a theoretical model based on layered models of ventilation flows introduced by Linden, Lane-Serff & Smeed (1990). The model predictions are compared with the laboratory experiments, and used to determine the dependence of these parameters on the cooling load, the ventilation rate and the properties of the cooling diffusers.

---

## 1. Introduction

After various attempts in the 19th century, including one by David B. Reed, an English scientist, who developed a system to humidify and ventilate the air supplied to the British House of Commons, air conditioning was invented by Willis Haviland Carrier. Carrier had his first patent ‘Apparatus for Treating Air’ (U.S. Patent 808897) granted in 1906, but it was Stuart H. Cramer, a textile engineer, who first used the term ‘air conditioning’ in a 1906 patent claim. Cooling for human comfort, rather than industrial need, began in 1924, in the J.L. Hudson Department Store in Detroit, Michigan. Air conditioning of apartments and homes began during the 1930s. In 1939, Packard Motors introduced air-conditioning units for cars. Currently, approximately 10% of all energy use in the United States is used for heating and cooling buildings. On a hot summer day in Los Angeles the amount of energy used in cooling buildings exceeds that used by transport! In many large cities the peak energy demand for cooling outstrips the supply. Building energy use is also a major contributor to CO<sub>2</sub> emissions.

Over the past 20 years or so architects, designers and engineers have become increasingly concerned with this energy use, and have sought ways to make buildings more energy efficient. Writing in the *Economist*†, Sir Norman Foster pointed out the implications on energy use and greenhouse gas emissions with increasing industrialization of India and China. New buildings, particularly in Europe but also in the US, are being designed with energy efficiency as a major consideration. There are many aspects to sustainability and energy efficiency of buildings, and a fluid dynamicist can contribute to the design of efficient heating and cooling systems. In many parts of the world, efficient cooling represents the main challenge and it is this aspect that we address in this paper.

The tendency for hot air to rise means that the air in a space is usually stably stratified,

† Special issue December 2004, *The World* in 2005, p126

with the warmest air at the ceiling. Conventional air conditioning systems supply cool air at the ceiling as forced, negatively buoyant jets. These jets fall to the floor, driven both by their initial momentum and by their negative buoyancy, and tend to mix the air within the space, minimizing the vertical stratification. The average temperature  $T_R$  of the air within the space and the ventilation rate  $Q$  are

$$T_R = T_S + \frac{\mathbf{H}}{Q\rho C_p} \text{ or } Q = \frac{\mathbf{H}}{\rho C_p(T_R - T_S)}, \quad (1.1)$$

where  $T_S$  is the supply temperature,  $\mathbf{H}$  is the heat flux of the internal gains within the space,  $\rho$  and  $C_p$  are the density and specific heat at constant pressure of air, respectively. Thus for a given supply temperature  $T_S$ , the minimum flow rate corresponds to the maximum return temperature  $T_R$ , and *vice-versa*. In a conventional overhead system the return temperature is the same as the space temperature, but if stratification is allowed it is possible for the return temperature to be larger than the space temperature. Thus a system that produces stratification provides the potential for removing the heat load at a lower ventilation rate, thereby reducing fan power, or using a larger supply temperature  $T_S$ , thereby reducing the chiller load.

Thus, one way to increase the efficiency of an air-conditioning system is to allow the air to stratify. This can be achieved by displacement ventilation where the cool, supply air is delivered at low velocities at the bottom of the space. The supply air spreads out across the floor, and the warm air is ‘displaced’ upwards and out of the space through return vents in the ceiling. Both the stratification and the return temperature are maximized in this case, and only the lower occupied zone is cooled. Provided some of this heated air is exchanged with cooler outside air, then, effectively, a fraction of the internal gains, rising as thermal plumes from sources within the space, are not cooled. Depending on the

local climate, energy savings can be as much as 40% over conventional air-conditioning systems (Bauman 2004).

The stratification within the space, while essential for realizing the energy savings, can potentially be uncomfortable. Individuals exposed to significant temperature variations over their bodies, experience discomfort. The industry standard (ASHRAE *Standard* 55–1992) recommends that temperature gradients be less than 1.9 K over 1 m. Recent work (Brager, Paliaga & de Dear 2004) suggests that this recommendation is too restrictive, and that humans can tolerate larger variations over the body, provided no part is excessively hot or cold. Irrespective of the particular values for tolerable temperatures, it is clear that a ventilation system that seeks to create significant stratification may have a negative impact on occupant comfort. In displacement systems, for example, the presence of cool air at floor level can be a cause of discomfort. Under floor air distribution (UFAD) is a ventilation strategy that attempts to improve comfort while retaining significant energy efficiencies over convective systems. UFAD uses a raised-access floor to create a plenum, into which conditioned air is supplied from the chiller. This air enters the space through vents, called ‘diffusers’, located in panels in the floor. The flow from a diffuser is an upward negatively-buoyant turbulent jet. This jet rises until its vertical momentum reduces to zero, after which it reverses and falls towards the floor. The height at which the flow reverses is known as the diffuser ‘throw’, and depends on the temperatures of the air in the plenum and the space, the initial momentum of the flow through the diffuser and the specific geometry of the diffuser. As in both the conventional and displacement systems, the return vents on the ceiling extract the hot air from the upper region.

The diffuser flows are designed to be turbulent, and air is entrained into the jet as it rises. When the flow reverses, it also continues to entrain and mix the air within the space. In particular, during its descent, the diffuser flow carries warm air downwards

from the upper part of the space, thereby increasing the temperature near the floor. This process reduces the stratification compared to that found in a pure displacement system, and provides a compromise between energy efficiency and thermal comfort.

The first UFAD system was introduced in the 1950s to cool a computer room (Grahl 2002). The massive amount of cooling and air conditioning required by mainframe computers created the need for a modular cooling system. Currently, UFAD is increasingly being installed in office buildings, where cooling loads are relatively small. Typically, in an open-plan environment, many diffusers are located in the floor, in order to provide localised cooling. Occupants can open or close diffusers near their work space, and this ‘local control’ is a popular feature. The use of modular panel floors allow the diffuser arrangements to be reconfigured easily, giving flexibility to the use of the space. The plenum itself also provides space to run cabling and other services under the floor, and avoids the need for false ceilings.

There is also a perceived improvement in air quality compared to a conventional overhead system. The plumes from the heat sources entrain pollutants from the lower part of the space and carry them to the upper, unoccupied part. Thus occupants are surrounded by relatively unpolluted supply air – rather like being washed in an inverted shower – as compared to a conventional mixing system in which pollutants are mixed throughout the space – like sitting in a bath.

As the above discussion shows, the optimal operation of a UFAD system involves a delicate balance between the stratification needed for energy efficiency while retaining thermal comfort. However, because the technology is in its infancy, engineers and designers lack information and experience to design UFAD systems, and standardized methods and guidelines are under development. The UFAD design guide by Bauman (2004) is the first, and only, design book so far. Furthermore, designers need tools with which they can

calculate the potential energy savings of a UFAD system when it is installed in a building. For conventional HVAC systems these calculations are made by running a thermal simulation program. In these programs it is assumed that each space within a building is well mixed, and the heat balances are calculated within each individual space, which is characterized by a single temperature, due to convective, conductive and radiative exchanges with the surfaces in the space. Since energy-efficient systems require stratification, these programs are unable to capture the energy savings, and there is a need to extend these simulation programs to include stratification. Typically, building simulation programs are run for whole buildings, which may consist of many tens of interior spaces, with two or more years of weather data, with a time step of 10 minutes. Consequently, the inclusion of stratification must be simple or the computational overhead will be too large.

Apart from empirical ‘rule-of-thumb’ calculations, the simplest approach is to use zonal or nodal models (Li 1993, Rees & Haves 2001, Musy, Winklemann & Wurtz 2002). However, there is no clear basis on which to assign zones or nodes to physical space, and much is left to the skill and judgement of the modeller. Our approach is a form of zonal model, except that the zones (the layers, plumes and jets) and the exchanges between them, are determined by the internal dynamics of the system.

Previous studies have used a zonal approach to model UFAD systems. Ito & Kakamura (1993) modelled the mixing process of the discharged air as two regions: a mixed region in the lower part of the room, and a ‘piston-flow’ region in the upper part. Consequently, the lower mixing zone height is only affected by the buoyancy and momentum of the diffuser. Zhang (2001) applied a room air stratification model similar to that of Ito & Nakahara (1993), with two regions in the ventilated space, and included the effect of

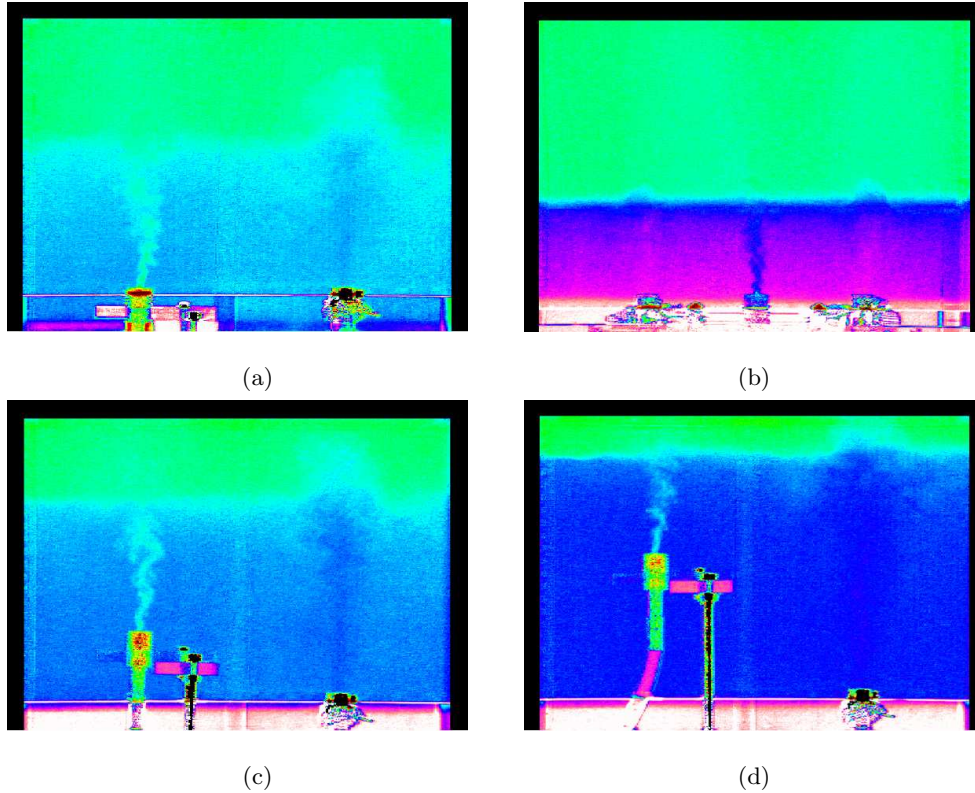


FIGURE 1. False colour images of the experiments. (a) The basic case of one heat source and a single diffuser. (b) One heat source and two diffusers. (c) An elevated heat source at  $1/4H$ . (d) An elevated heat source at  $1/2H$ . The effect of additional diffusers, for a given total flow rate, is to reduce the interface height and reduce the lower layer temperature, while raising the heat source above the floor raises the interface and reduces the lower layer temperature.

thermal plumes. However, his assumption that the lower zone height was not influenced by the momentum of the diffuser flows, does not agree with observations.

Lin & Linden (2005) conducted laboratory simulations of the flow patterns of a simplified UFAD in a ventilated room, in which a single heat source and a single cooling diffuser are both located at the floor level. This case is illustrated in figure 1 (a), which shows a false colour image of the flow. They also developed a theoretical model for a floor-positioned single-heat source and single-diffuser UFAD system, which was compared with their experiments. Lin & Linden (2005) showed that the entrainment of warmer air from

the upper zone by the diffuser flow is a crucial feature of the performance of a UFAD system.

In this paper, we present experiments and develop a theoretical model of a UFAD system containing multiple cooling diffusers (figure 1 (b)) and elevated heat sources (figures 1 (c) and (d)). The theoretical model of multiple diffusers and that of an elevated heat source is developed in § 2 and the laboratory experiments are described in § 3. In § 4 the comparisons of the theoretical predictions and experimental measurements are presented. The main conclusions of our work are discussed in § 5.

## 2. The theoretical model

### 2.1. *Plume & fountain equations*

A plume, with a given buoyancy flux  $B$  originating from a point source, is used to represent the flow above a heat source. The flow is characterised by the mean radius  $b$ , the vertical velocity  $w(r, z)$  and the reduced gravity  $g' = g(\rho_o - \rho)/\rho_s$ , or  $g' = g(T - T_o)/T_s$  for an ideal gas, where  $\rho_s$  is the reference density,  $\rho_o$  and  $\rho$  are the densities in the ambient fluid and in the plume respectively, with the absolute temperature  $T$  similarly defined. Consequently, in the following, values of  $g'$  are proportional to temperature differences relative to a reference temperature. Further, since  $T - T_s \ll T_s$  in room ventilation, the Boussinesq approximation is valid.

The entrainment assumption by Morton, Taylor, & Turner (1956) and Morton (1959), that the rate of entrainment at the edge of a plume is proportional to the vertical velocity at that height, is applied to model flow in the plume. ‘Top-hat’ distributions of vertical velocity,  $\bar{w}$ , and reduced gravity,  $\bar{g}'$ , in which the values are taken as constant cross-sectional averages across the plume, and zero outside, are used. When the environment



density  $\rho_o$  is constant, the governing equations for a plume can be quantified using the entrainment equations of Morton *et al.* (1956)

$$\frac{d}{dz}(b^2\bar{w}) = 2\alpha b\bar{w}, \quad \frac{d}{dz}(b^2\bar{w}^2) = b^2\bar{g}', \quad \frac{d}{dz}(b^2\bar{w}\bar{g}') = 0, \quad (2.1)$$

where  $\alpha$  is the entrainment coefficient of the plume. These equations have analytic solutions and, in particular, the volume flux  $Q$  in the plume is given by

$$Q = C(Bz^5)^{1/3}, \quad (2.2)$$

where  $C = \frac{6}{5}\alpha(\frac{9}{10}\alpha)^{\frac{1}{3}}\pi^{\frac{2}{3}}$ . The entrainment rate  $\alpha$  of the plume was chosen to be 0.117, consistent with the values reported by Rouse, Yih & Humphreys (1952), Papanicolaou & List (1988) and Hunt & Linden (2001), giving  $C = 0.142$ .

The flow from the diffusers takes the form of a negatively-buoyant turbulent jet – colloquially called a fountain – which rises a certain height until the negative buoyancy reduces its upward momentum flux to zero. The flow then reverses and falls down in an annular region outside the rising jet (Turner 1966).

Bloomfield & Kerr (2000) derived a set of non-dimensional variables based on the initial source volume flux  $Q_0$ , momentum flux  $M_0$  and buoyancy flux  $F_0$  of the fountain

$$\begin{aligned} \tilde{z} &= M_0^{-\frac{3}{4}}F_0^{\frac{1}{2}}z, \quad \tilde{b} = M_0^{-\frac{3}{4}}F_0^{\frac{1}{2}}b, \\ \tilde{u} &= M_0^{\frac{1}{4}}F_0^{-\frac{1}{2}}\bar{w}, \quad \tilde{g}' = M_0^{\frac{5}{4}}F_0^{-\frac{3}{2}}\bar{g}'. \end{aligned} \quad (2.3)$$

Then, the dimensionless fluxes of volume  $\tilde{Q} = \tilde{b}^2\tilde{u}$ , momentum  $\tilde{M} = \tilde{b}^2\tilde{u}^2$ , and buoyancy  $\tilde{F} = \tilde{b}^2\tilde{u}\tilde{g}'$ , and (2.1) take the non-dimensional form for a fountain

$$\frac{d}{d\tilde{z}}(\tilde{b}^2\tilde{u}) = 2\alpha_f\tilde{b}\tilde{u}, \quad \frac{d}{d\tilde{z}}(\tilde{b}^2\tilde{u}^2) = \tilde{b}^2\tilde{g}', \quad \frac{d}{d\tilde{z}}(\tilde{b}^2\tilde{u}\tilde{g}') = 0 \quad (2.4)$$

where  $\alpha_f$  is the entrainment coefficient of the fountain.

The starting conditions for the integration of equations (2.4) are defined at a height  $z_0 = 0$  of the fountain source. Then, the non-dimensional source conditions are  $\tilde{Q}(\tilde{z}_0) = M_0^{-\frac{5}{4}} F_0^{\frac{1}{2}} Q_0$ , and  $\tilde{M}(\tilde{z}_0) = 1$ . In a uniform environment, the buoyancy flux  $\tilde{F}$  is unchanged from its value at the source, which gives  $\tilde{F}(\tilde{z}_0) = -1$ . We have used a routine, based on a fourth-order Runge-Kutta method, to solve the dimensionless governing equation numerically.

Based on our experimental observations (see §4), we assume a two-layer stratification is produced in the steady state. The interface separates a lower layer of reduced gravity  $g'_1 = g \frac{\rho_1 - \rho_s}{\rho_s}$  from an upper layer of reduced gravity  $g'_2 = g \frac{\rho_2 - \rho_s}{\rho_s}$ . The penetrative entrainment by a turbulent fountain through an interface is crucial to the performance of the UFAD system. Lin & Linden (2005) assumed that the penetrative entrained volume flux  $Q_e$  across the density interface is proportional to the impinging volume flux  $Q_i$  at the density interface

$$Q_e = Q_i E, \quad (2.5)$$

where  $E$  is the penetrative entrainment rate. This penetrative entrainment brings upper zone warm fluid across the interface to the lower occupied zone. The penetrative entrainment rate across the density interface is a function of the local Richardson number  $Ri$  at the interface, i.e.  $E = E(Ri)$ , where  $Ri = \frac{(g'_2 - g'_1) b_i}{w_i^2}$  (Baines 1975). Here,  $w_i$  and  $b_i$  are the vertical velocity and the radius, respectively, of the fountain at the density interface position and  $g'_2 - g'_1$  is the reduced gravity step at the interface. This form is similar to that proposed by Kumagai (1984) who considered the impingement of a plume on an interface. The entrainment rate  $E$  was determined from experiments.

At low interface stabilities (low  $Ri$ ), Lin & Linden (2005) found a constant  $E$ . Our,

more extensive, experiments suggest that at higher interface stability the entrainment rate decreases and we found (Liu 2005)

$$E = \begin{cases} 0.6 \pm 0.1, & \text{if } Ri \leq 8, \\ 4.8 Ri^{-1} \pm 0.1, & \text{if } Ri > 8. \end{cases} \quad (2.6)$$

### 2.2. Fixed heat load and total ventilation rate

In this, and the next section, we consider the effect of distributing the ventilation air between different numbers of diffusers. Here we consider the effect of distributing the same ventilation air among different diffusers. This calculation is important in the design of a UFAD system, where the optimal number of diffusers for a given space needs to be decided. Consider a single UFAD space, with a constant heat load and total ventilation rate, at steady state. At an interface height  $h$ , the plume and each fountain carry a volume flux  $Q_p$  and  $Q_i$ , respectively. The plume volume flux is given by (2.2) at  $z = h$ . An amount of upper layer fluid  $Q_e$  is entrained back into the lower layer by the fountain above each cooling diffuser, leaving a net flow rate  $Q$ , where  $Q$  is the total ventilation rate, through the system. We begin by supposing that the ventilation flow  $Q$ , originally supplied through one diffuser is now divided equally between two diffusers, as shown in figure 2(a). Since the momentum flux from an individual diffuser is proportional to  $Q_f^2$ , the momentum flux for each diffuser is one-quarter of that of a single diffuser carrying the same ventilation flow. Hence, as more diffusers are opened, the fountain from each diffuser is weaker and the total entrainment of upper layer fluid into the lower layer will be reduced.

We assume that the two cooling diffusers are identical. Since the flow through them is

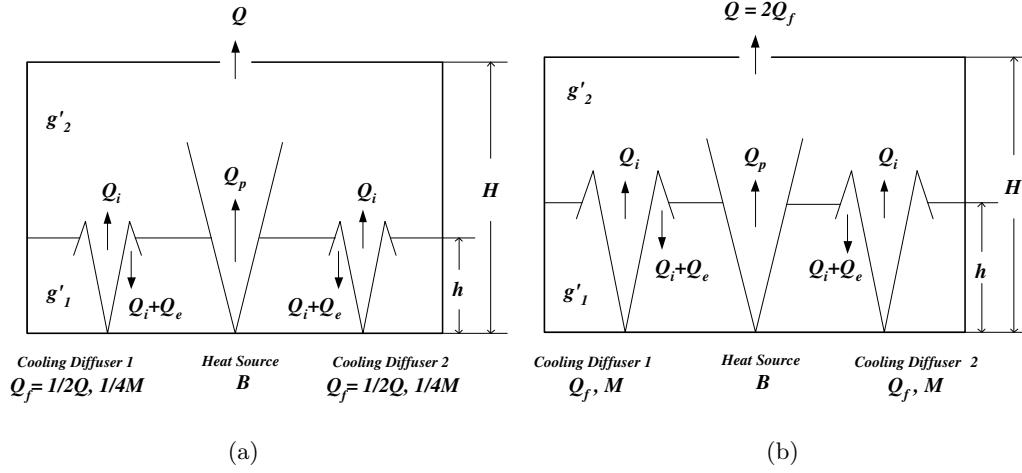


FIGURE 2. A UFAD model with a single heat source and two equal cooling diffusers (a) with fixed ventilation flow rate; (b) with constant underfloor pressure.

driven by the (assumed spatially uniform) plenum pressure, the flow from each diffuser is also the same †.

Since the vertical transfer of fluid across the stable interface can only take place within the plume, in steady state, conservation of volume flux gives

$$Q_p = 2\left(\frac{1}{2}Q + Q_e\right). \quad (2.7)$$

In a steady state, the buoyancy flux carried out through the exit is equal to the buoyancy flux produced in the space by the heat source  $B$ , so that

$$g'_2 = \frac{B}{Q}, \quad (2.8)$$

According to (2.8), the steady-state reduced gravity  $g'_2$  of the upper layer and, therefore, the return temperature (assumed here to be the same as the upper layer temperature)

† Some commercial diffusers can be controlled by individual occupants, e.g. by partially closing the vent. In this case the different flows above each diffuser produces horizontal variations that are beyond the scope of this study.

depends only on the total heat load and the total ventilation rate for the space, and is independent of the number of (and the properties of the) cooling diffusers.

The reduced gravity of the lower layer  $g'_1$ , is determined by the fluid entrained by the two cooling diffusers from the upper layer. We assume that this fluid is mixed uniformly throughout the lower layer, so that

$$g'_1 = \frac{g'_2 Q_e + g'_f \frac{1}{2}Q + g'_1 (Q_i - \frac{1}{2}Q)}{Q_e + \frac{1}{2}Q + (Q_i - \frac{1}{2}Q)} = \frac{g'_2 Q_e}{Q_e + \frac{1}{2}Q}. \quad (2.9)$$

where  $g'_f$  is the buoyancy of the diffuser flow. In the following, the reference density and is chosen so that  $g'_f = 0$ , and all temperatures are referenced to the supply temperature.

We can readily generalize to  $n$  equal cooling diffusers, in which case (2.7) becomes

$$Q_p = n\left(\frac{1}{n}Q + Q_e\right), \quad (2.10)$$

and the lower layer reduced gravity is given by

$$g'_1 = \frac{g'_2 Q_e}{Q_e + \frac{1}{n}Q}. \quad (2.11)$$

Hence

$$\frac{g'_1}{g'_2} = \frac{nQ_e}{nQ_e + Q}. \quad (2.12)$$

Since the upper layer buoyancy (the return temperature)  $g'_2$  does not change with  $n$ , and  $Q_e$  decreases due to the lower momentum of each fountain as  $n$  increases, the lower layer temperature  $g'_1$  will decrease as  $n$  increases. The total entrainment  $nQ_e \rightarrow 0$ , even if  $n \rightarrow \infty$ , since  $Q_e$  increases with the momentum flux of the fountain  $M \propto n^{-2}$ , so that  $Q_e$  decreases more quickly than  $n$  increases. Therefore, according to (2.12)  $g'_1 \rightarrow 0$  as  $n \rightarrow \infty$  and the lower layer temperature equals the supply temperature. This limit recovers displacement ventilation in which the supply air enters the space without mixing.

*2.3. Fixed heat load and underfloor pressure*

In this section we continue the discussion of the effect of different numbers of diffusers. Here we are considering a functioning UFAD system with the underfloor plenum held at a fixed pressure and consider the effect of the occupants opening or closing diffusers to change the total number in operation. In this case each diffuser has the same pressure drop across it and delivers the same amount of supply air  $Q_f$ . Then, as more diffusers are opened, the total amount  $Q$  of air supplied to the room increases as  $Q = nQ_f$ , while the strength of each diffuser flow remains constant. Figure 2(b) shows a UFAD system consisting of a heat source and two cooling diffusers, when the heat load and underfloor pressure are constant.

Mathematically, (2.10), (2.8) and (2.11) become

$$Q_p = n(Q_f + Q_e), \quad (2.13)$$

$$g'_2 = \frac{B}{Q}, \quad (2.14)$$

$$g'_1 = \frac{g'_2 Q_e}{Q_e + Q_f}. \quad (2.15)$$

These equations show that, as more diffusers are opened and  $n$  increases,  $Q_p$  increases and the interface position is raised, and the upper layer buoyancy (the return air temperature) decreases, since  $g'_2 \sim \frac{1}{n}$ . Further, since  $Q_f$  is constant with  $n$ , the lower zone temperature  $g'_1$  gets cooler as  $g'_2$  decreases. At the limit when  $n \rightarrow \infty$ , according to (2.14),  $g'_2 \rightarrow 0$ , and  $g'_1 \rightarrow 0$  results from (2.15). The two-layer stratification disappears, and a uniform temperature at the supply air temperature is obtained. In this case, the limit

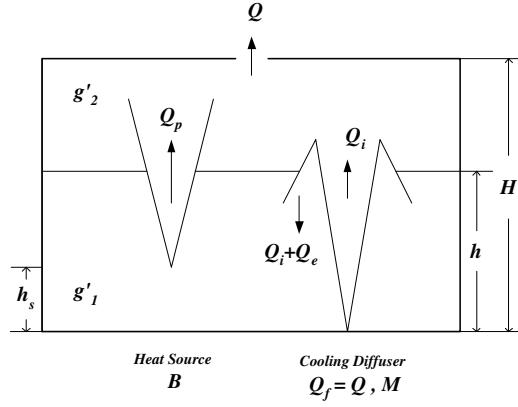


FIGURE 3. A UFAD system with a heat source above the floor

as  $n \rightarrow \infty$  is to mixing ventilation caused by the large ventilation rate, with consequent loss of energy-efficiency. Such a system is said to be ‘over-aired’.

#### 2.4. An elevated heat source

Heat sources, such as lamps or computers, are often not located on the floor. Even the thermal effect of a human, may be considered as a plumes rising from the upper part of the body, rather than from the feet. Therefore, it is of importance to study the effects of vertical locations of a heat source in a UFAD system. In this section, we introduce the vertical height  $h_s$  of the plume source as a parameter.

Volume conservation implies

$$Q_p = Q + Q_e. \quad (2.16)$$

Buoyancy conservation implies the reduced gravities for the upper and lower layers are

$$g'_2 = \frac{B}{Q} \quad (2.17)$$

and

$$g'_1 = \frac{g'_2 Q_e}{Q_e + Q}. \quad (2.18)$$

As discussed in §2.1, the volume flux  $Q_p$  in the plume at the density interface is related

to the buoyancy flux  $B$  of the heat source and the distance of the interface from the source origin, which now is  $h - h_s$ , and

$$Q_p = C [B (h - h_s)^5]^{1/3}. \quad (2.19)$$

The effect of raising the heat source off the floor is to decrease the length of the plume over which entrainment can occur, and so the interface rises to provide the required volume flux  $Q_p$ , compared to the interface height for a heat source on the floor. Since, changing the vertical position of the heat source does not change  $B$  or  $Q$ , the temperature of the upper layer remains the same. Further, since the velocity at the diffuser decreases with height, the stability of the interface increases as  $h_s$  increases. Consequently, the interfacial Richardson number  $Ri$  increases, and the entrainment rate  $E$  decreases. Therefore, the diffuser flow brings less warm fluid to the lower cool layer, i.e.  $Q_e$  is smaller. According to (2.18) the lower cooled zone temperature  $g'_1$  drops.

### 3. The experiments

In our experiments, a salt-solution plume source represents a heat source, and fresh-water jets simulate cooling diffusers. Salt solution has a negative buoyancy force in fresh water, in contrast to the heat sources in a building. Therefore, the geometry of the experiments are inverted from a real UFAD system. However, for Boussinesq flows, this reversal of the direction of the buoyancy force is unimportant to the dynamics. In §4, all the results are presented with an inverted geometry compared to the laboratory, so that they correspond to the ventilation orientation.

Experiments were conducted in two, clear rectangular plexiglas tanks (tank #A with cross-sectional area 30.6 cm  $\times$  15.3 cm and 30.6 cm deep, and tank #B with the dimensions of 58.5 cm long, 28 cm wide and 58.5 cm deep) filled with fresh water. The



salt solution was colored with a known concentration of dye for flow visualization and quantitative measurement. The dyed salt solution and transparent fresh water were supplied to the sources from a constant-head, gravity-fed system. Flow rates were controlled by calibrated flow meters. The circular plume nozzle (diameter  $D = 0.5$  cm) used in the experiments, was designed by Dr. Paul Cooper, Department of Engineering, University of Wollongong, NSW, Australia. The fountain source nozzles in the experiments are plexiglas pipes (1.27 cm in diameter) with a piece of fine mesh (aperture size about 0.1 cm $\times$ 0.1 cm) placed over the opening to produce vertically directed turbulent fountains. All nozzles are separated from one another horizontally by about 6 ~ 8 cm, so that the plume and fountains develop independently. Discussions of interacting jets and plumes, of relevance when a diffuser is located close to a heat source or when heat sources are close together, can be found in Hunt, Linden & Cooper (2001) and Kaye & Linden (2004). A siphon pipe, continuously extracting fluid from the bottom of the tank during the experiments, simulates the return vent on the ceiling in a real UFAD system.

All experiments were recorded by capturing images with a CCD camera. The attenuation of light, from a light source placed behind the tank, by the tracer dye added to the salt solution was analyzed by *DigImage* (Dalziel 1992-1998), to determine the local density, averaged across the width of the tank. The density distribution in the tank was verified by withdrawing small samples of fluid, typically 3 ml, at 1 cm intervals in height with a syringe. The density was measured by an Anton Paar DMA 5000 density meter, accurate to  $10^{-5}$  g cm $^{-3}$ . The discrepancy between these two measuring methods, which is within 5% of the initial salt concentration, comes mainly from the fact that the measurements were taken at different times. The fluid samples were withdrawn after each experiment was completed, while the light attenuation was extracted from the video taken during the experiments. Some other factors, such as the variability of the

---

Exp. No.	$B$ (cm <sup>4</sup> sec <sup>-3</sup> )	$M$ (cm <sup>4</sup> sec <sup>-2</sup> )	$Q_f$ (cm <sup>3</sup> sec <sup>-1</sup> )	No. of Diffusers	Tank Label
1	70.11	142.02	13.43	1	A
2	71.76	35.35	6.7	2	A
3	69.28	181.92	15.2	1	A
4	68.22	45.48	7.6	2	A
5	69.28	58.24	8.6	2	A
6	69.30	74.09	9.7	2	A
7	70.11	26.31	5.0	3	B
8	70.95	44.46	6.5	3	B

---

TABLE 1. 8 different experimental conditions for the multiple diffusers experiments.  $B$  is the buoyancy flux of the heat source,  $M$  and  $Q_f$  are the momentum fluxes and the volume fluxes of each cooling diffuser.

salt solution density and the background lighting, also contribute to the discrepancy. All experimental measurements agree with the theoretical predictions, within 10% error.

Experiments were carried out with buoyancy fluxes  $B$  of the plume around 70 cm<sup>4</sup>s<sup>-3</sup> and the momentum fluxes  $M$  of the fountains varied from 25 to 243 cm<sup>4</sup>s<sup>-2</sup>. The plume and fountains were observed to be fully turbulent. The experimental conditions for each run with  $h_s = 0$  were summarized in Table 1. The effects of an elevated heat source ( $h_s \neq 0$ ) was investigated by changing the vertical position of the heat source for the parameters of Exp. 3.

The plume, produced by adding salt solution, is not the ‘ideal’ plume of Morton *et al.* (1956) since it has finite volume flux  $Q_s$  and momentum flux  $M_s$  at the source. A plume rising from a heat source (unless it is a convector heater with a fan, say) has  $Q_s = 0$  and  $M_s = 0$ . The effects of the non-ideal plume initial conditions can be accounted for by calculating a virtual origin, which is a height of the origin of an equivalent ideal plume

that would have the actual (non-zero)  $Q_s$  and  $M_s$  at the physical location of the real plume source. The virtual origin of the plume  $z_v$  for our experiments, determined by the method given in Hunt & Kaye (2001), ranges from 0.99 to 1.3 cm, which is small compared with the depths of the tanks.

The second effect of representing a heat source by a finite volume flux  $Q_s$  of salt solution with buoyancy  $g'_s$ , is that the buoyancy flux is  $B = Q_s(g'_s - g'_1)$ . Since  $g'_1$  is not known *a priori*, the buoyancy flux needs to be calculated at the end of the experiment. Then the volume flux in the plume  $Q_p$  at the density interface, is given by

$$Q_p = C [B (h + z_v)^5]^{1/3}. \quad (3.1)$$

Finally, the finite plume-source volume flux contributes to the overall volume flow through the tank. Hence,  $Q = nQ_f + Q_s$ . In the experiments  $Q_s \approx 0.85 \text{ cm}^3/\text{s}$ , which is less than 6% of the total volume flow rate through the tank, and always significantly less than  $Q_p$  at the interface. Thus, this small addition of volume does not affect the flow significantly, and we take it into account (by inclusion through conservation equations) in all comparisons between the theory and the experiments.

The fountains also do not have ideal point sources assumed in the model of Bloomfield & Kerr (1998). Consequently, we carried out a separate series of experiments, described in Liu (2005), in order to characterize the flow from the sources used in our experiments. We found that the most appropriate value for the entrainment coefficient was  $\alpha_f = 0.075 \pm 0.015$ , and this value is used in the numerical calculations of the fountain flow.

## 4. Experimental results & comparisons with the model predictions

### 4.1. Effects of multiple diffusers

We have carried out the experiments with one or two diffusers in the smaller tank #A, and three diffusers in the larger tank #B. All these experiments have a single plume on the floor. In the following graphs, solid lines or ‘o’ indicate the theoretical predictions, ‘\*’ are the experimental measurements analyzed by *DigImage*, and ‘.’ are the measurements of fluid samples. We define a dimensionless height

$$\hat{z} = \frac{z}{C^{-3/5}Q^{3/5}B^{-1/5}}, \quad (4.1)$$

where  $C = 0.142$  is the universal plume constant and a dimensionless buoyancy

$$T/T_R \equiv \hat{g}' = \frac{g'Q}{B}. \quad (4.2)$$

Hence,  $\hat{h} = 1$  corresponds to the interface height at which all the ventilation flow is carried by the plume (2.2), and  $\hat{g}' = 1$  corresponds to the return temperature given by (2.8).

Exp. 1 and Exp. 2 (Table 1) have almost the same plume buoyancy fluxes and total ventilation rate  $Q$ , while Exp. 2 has two cooling diffusers which split the total volume flux of the single diffuser in Exp. 1. In figure 4(a), we see that a two-layer temperature stratification forms in both cases. The upper layer temperature remains approximately the same, at the predicted return temperature  $\hat{g}' = 1$ , (2.8). When the ventilation flow is split between two diffusers, the lower layer temperature and the interface height both decrease. The theoretical predictions of the upper layer temperature and the interface position have the same behaviour, and they agree well with the experimental data. However, the lower layer in Exp. 2 is more stratified than in Exp. 1 because, in the experiments, it

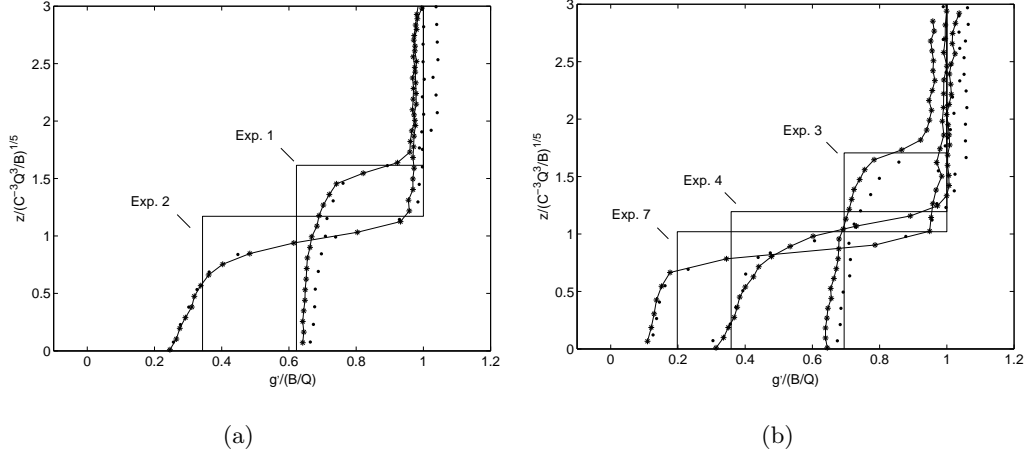


FIGURE 4. Buoyancy profiles obtained at steady state with multiple diffusers with fixed heat load and ventilation rate. The height is made dimensionless by the height scale  $C^{-3/5}Q^{3/5}B^{-1/5}$  based on the total ventilation rate and buoyancy flux, and the buoyancy by the buoyancy scale  $B/Q$ . (a) Exp. 1 with a single diffuser and Exp. 2 with two diffusers; (b) Exp. 3 with one diffuser, Exp. 4 with two diffusers and Exp. 7 with three diffusers.

is difficult to obtain exactly the same flow from each diffuser. Consequently, one diffuser might entrain more upper warm layer fluid than the other, thereby producing slightly different downward heat fluxes at each diffuser and producing some weak stratification. However, this was always observed to be a relatively small effect, and the density in the lower layer is approximately uniform. The experimental data confirm the theoretical predictions in that the interface height and the lower layer temperature have both decreased.

Note further that the dimensionless interface height in Exp. 1 is approximately 1.6, and this value is reduced to approximately 1.2 in Exp. 2. Values above the theoretical value of 1, at which all the ventilation flow is carried by the plume, are a result of entrainment of upper layer fluid back down into the lower layer. Further, since  $Q \sim h^{5/3}$ , this change shows that splitting the ventilation flow between the two diffusers reduces the total entrainment by a factor of about 7, which is caused by a reduction in the

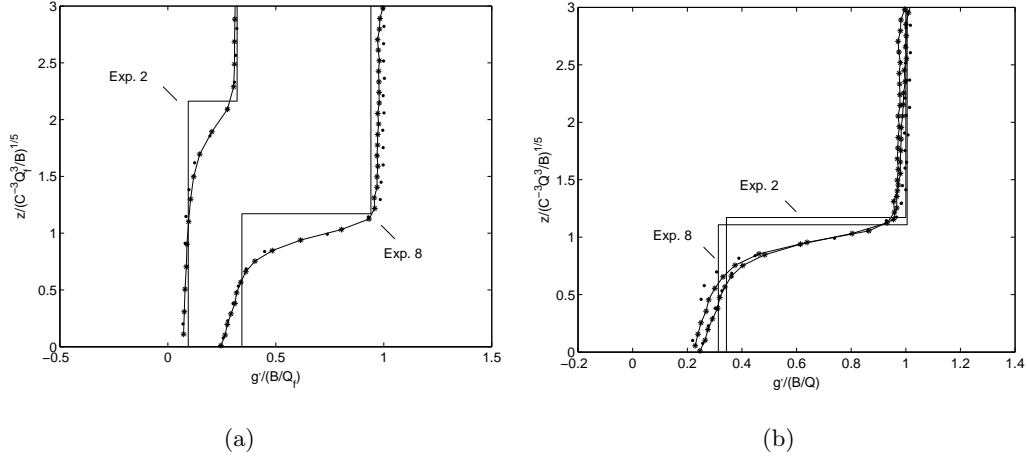


FIGURE 5. Dimensionless buoyancy profiles obtained at steady state with multiple diffusers for fixed heat load and underfloor pressure; Exp. 2 with 2 diffusers and Exp. 8 with 3 diffusers. (a) The buoyancy non-dimensionalized with the volume flux  $Q_f$  from each diffuser. (b) The buoyancy non-dimensionalized with the total ventilation volume flux  $Q$ .

momentum flux of each diffuser to about one-quarter of that of a single diffuser. This sensitivity to the diffuser flow shows the importance of the penetrative entrainment from the upper layer. The reduction in the lower layer temperature is also a consequence of the decreased total entrainment from the upper layer. Figure 4(b) shows the effect of changing the number of diffusers from 1 to 3, at the same heat load and ventilation flow rate. The same trends for variations in temperature in both layers and the interface position with increasing number of diffusers were observed and there is good agreement with the theoretical model.

In every case, the interface position measured in the experiments falls below the theoretical value. The entrainment rate  $E$ , given by (2.6), is tuned to the case of a single diffuser and, as can be seen in these figures, the agreement is best for these cases (Exp. 1 and Exp 3). The lower layer temperature is well predicted in each case.

The case where the underfloor pressure remains fixed, so that increasing the number of diffusers increases the total ventilation flow rate  $Q$ , is shown in figure 5, which compares

Exp. 2 and Exp. 8. The two experiments have almost the same buoyancy flux  $B$  from the heat source, and volume flux  $Q_f$  from each diffuser. In figure 5(a), the profiles are non-dimensionalised using  $B$  and  $Q_f$ , and as these are fixed, the changes in the profiles reflect those observed in the physical variables. We observe that, with increasing number of diffusers and, consequently, increasing  $Q$ , the temperature in both layers decreases and the interface height increases, as expected from the model described in §2.3. Quantitative agreement with the model is also found in this case. In figure 5(b), the profiles are non-dimensionalised by the total ventilation rate  $Q$ . In this case, the profiles tend to collapse on to a single curve. The use of  $Q$  ensures that the dimensionless return temperature  $\hat{g}'_2 = 1$ . The dimensionless occupied zone temperature  $\hat{g}'_1$  can be obtained by using (2.13), (2.14) and (2.15)

$$\hat{g}'_1 = \hat{g}'_2 \frac{Q_e}{Q_e + Q_f} = \hat{g}'_2 \left(1 - \frac{nQ_f}{Q_p}\right), \quad (4.3)$$

and the dimensionless interface height

$$\hat{h} = \frac{h}{C^{-3/5} (nQ_f)^{3/5} B^{-1/5}}. \quad (4.4)$$

Therefore, both  $\hat{g}'_1$  and  $\hat{h}$  are constant, if  $h \sim n^{3/5}$ , a result we will derive later.

The theoretical predictions of the dimensionless buoyancy profiles, for a fixed heat load with different numbers of cooling diffusers, are shown in figure 6. Figure 6(a) shows profiles for fixed total ventilation flow rate, but with the supply air divided equally between  $n$  diffusers, as discussed in §2.2. As we can see in this figure, the upper layer buoyancy (i.e. the return temperature) remains constant. When  $n = 1 \sim 4$ , the interface descends and the lower layer temperature decreases rapidly with increasing  $n$ . When  $n \geq 5$ , the effect of additional diffusers on the interface position and the lower layer

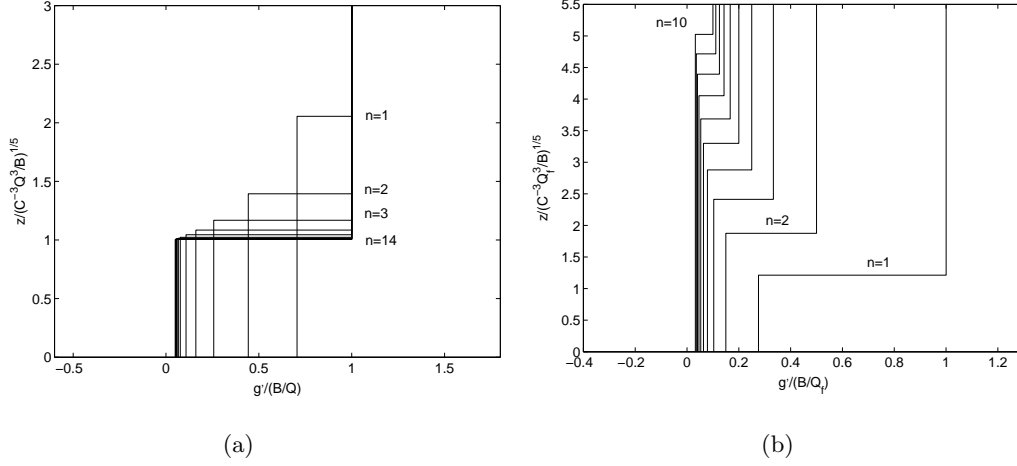


FIGURE 6. (a) Theoretical predictions for  $n$  equal cooling diffusers in the conditions of constant ventilation flow rate,  $n = 1, \dots, 14$ ; (b) Theoretical predictions for  $n$  equal cooling diffusers in the conditions of constant under floor pressure,  $n = 1, \dots, 10$ .

density is minimal. For these large numbers of diffusers, the entrainment of upper layer fluid becomes negligible, and the system operates as a displacement ventilation system with no appreciable mixing of the supply air. Hence, the lower layer temperature is at the supply temperature ( $g'_1 = 0$ ), and the interface height is that at which the plume carries the total ventilation rate ( $\hat{h} = 1$ ).

Figure 6(b) shows the buoyancy profiles given the same heat load and underfloor pressure, but with the total ventilation rate increasing with  $n$ , as discussed in §2.3. In this case, we observed a temperature drop in both layers, and a higher interface as  $n$  increases. In the limit of large  $n$ , the increase in the ventilation flow rate destroys the stratification, and mixing ventilation occurs.

In order to calculate the effects of changing the number of diffusers, we examine the two cases as  $n$  varies. Consider the case where the total ventilation flow rate is held fixed. Figure 7 shows (a) the dimensionless interface height  $\hat{h}$  and (b) the dimensionless buoyancy difference, plotted against  $n$ . As expected,  $\hat{h}$  decreases with increasing  $n$ , approaching the displacement limit  $\hat{h} = 1$  at large  $n$ , and the buoyancy difference increases



to the same limit for large  $n$ . For small values of  $n \leq 4$ ,  $\hat{h}$  and  $(\hat{g}'_2 - \hat{g}'_1)$  vary as  $n^{-0.52}$  and  $n^{0.9}$ , respectively, as  $n$  increases. In order to understand these trends we approximate the flows as follows.

We assume that the virtual origin of the plume  $z_v$  is small compared to the height of the interface  $h$ . From (3.1), for a fixed heat load,  $Q_p \sim h^{\frac{5}{3}}$ . Consider, first, the case when  $n$  is large, so that entrainment by the diffusers is weak, and  $nQ_e \ll Q_p$ . Then (2.10) reduces to  $Q_p = Q$ , and  $Q_p \sim h^{\frac{5}{3}}$  implies that the interface height is independent of  $n$  and  $\hat{h} = 1$ . On the other hand, when  $n$  is small,  $Q_e$  scales as  $\frac{1}{n}Q$ . As a first approximation, we further assume that the diffuser flow acts like a jet so that the momentum flux  $M$  of the fountain is conserved. Dimensional analysis shows that at each height  $z$ , the mean vertical velocity  $w$ , the radius  $b$  of the fountain, and the volume flux  $Q$  are given by

$$w \sim M^{\frac{1}{2}} z^{-1}, \quad b \sim z \quad Q \sim wb^2 \sim M^{\frac{1}{2}} z. \quad (4.5)$$

Hence, the volume flux of the diffuser flow and the Richardson number at interface are  $Q_i \sim h$ , and  $Ri \sim \frac{g' h^3}{M}$ , respectively.

At low  $Ri \leq 8$ ,  $E$  is constant so that  $Q_e \sim h$ , which implies that  $\hat{h} \sim n^{-1}$ . For a larger Richardson number,  $E \sim \frac{1}{Ri}$ , so  $Q_e \sim \frac{M^{\frac{3}{2}}}{g' h^2}$  and  $\hat{h} \sim n^{-\frac{1}{2}}$ . In the experiments,  $E$  is in the constant regime for small  $n$  and moves into the variable regime at larger  $n$  (see (2.6)). The observed power law  $-0.52$ , although based on a fit to very few points, is not inconsistent with this analysis.

The non-dimensional density difference is given as

$$\hat{g}'_2 - \hat{g}'_1 = \frac{Q}{Q_p}. \quad (4.6)$$

Therefore,  $(\hat{g}'_2 - \hat{g}'_1)$  is independent of  $n$ , at large values of  $n$ , as observed. With small  $n$ , depending on the interface  $Ri$ ,  $(\hat{g}'_2 - \hat{g}'_1) \sim n^{\frac{5}{3}}$  for small  $Ri$  and  $(\hat{g}'_2 - \hat{g}'_1) \sim n^{\frac{5}{8}}$  for large

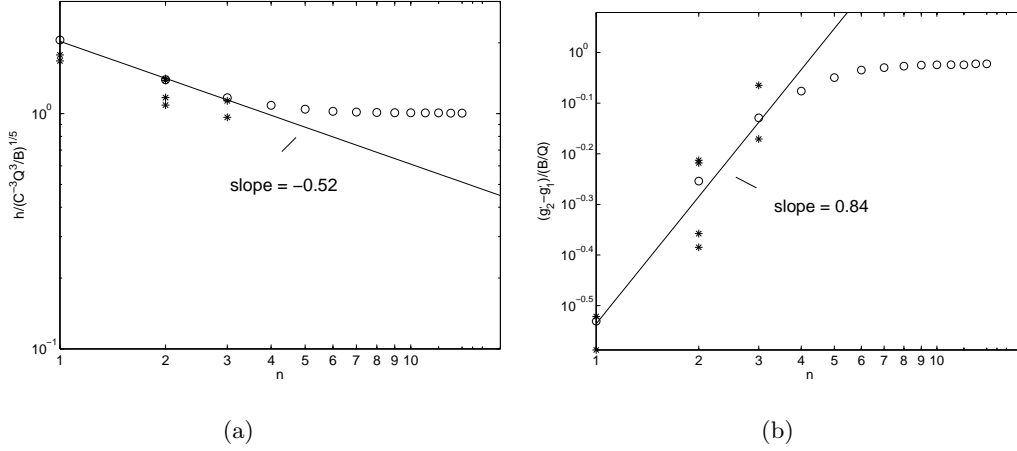


FIGURE 7. (a) The dimensionless interface height  $\frac{h}{(C^{-3}Q^3/B)^{1/5}}$  and (b) the non-dimensional density difference between two layers  $\frac{g'_2}{B/Q} - \frac{g'_1}{B/Q}$  plotted against the number of diffusers  $n$  when the total ventilation rate is fixed. The stars are the experimental results and the open circles are the results from the model.

$Ri$ , respectively. The observed power law 0.84 (figure 7(b)) is consistent with  $E$  varying from the constant regime to the variable regime when  $n$  increases.

We now turn to the case where the underfloor plenum pressure is held fixed. Since, in this case the flow across each diffuser is fixed, we replace  $Q$  by  $Q_f$  in (4.1) and (4.2), so that the dimensionless height is

$$\hat{z}_f = \frac{z}{C^{-3/5}Q_f^{3/5}B^{-1/5}}, \quad (4.7)$$

and a dimensionless buoyancy

$$\hat{g}' = \frac{g'Q_f}{B}, \quad (4.8)$$

so that  $\hat{g}'_2 = 1$  corresponds to the single-diffuser case ( $n = 1$ ), where  $Q_f = Q$ .

As before, when  $n$  is large,  $nQ_e \ll Q_p$ . Thus,  $Q_p = nQ_f$  from (2.13). Since  $Q_f$  is a constant,  $\hat{h} \sim n^{3/5}$ . If  $n$  is small,  $nQ_f$  and  $nQ_e$  are comparable. Then,  $Q_p = ncQ_f$ , where,  $c$  is a constant. So, again,  $\hat{h} \sim n^{3/5}$ . Consequently,  $\hat{h} \sim n^{3/5}$  for any number of

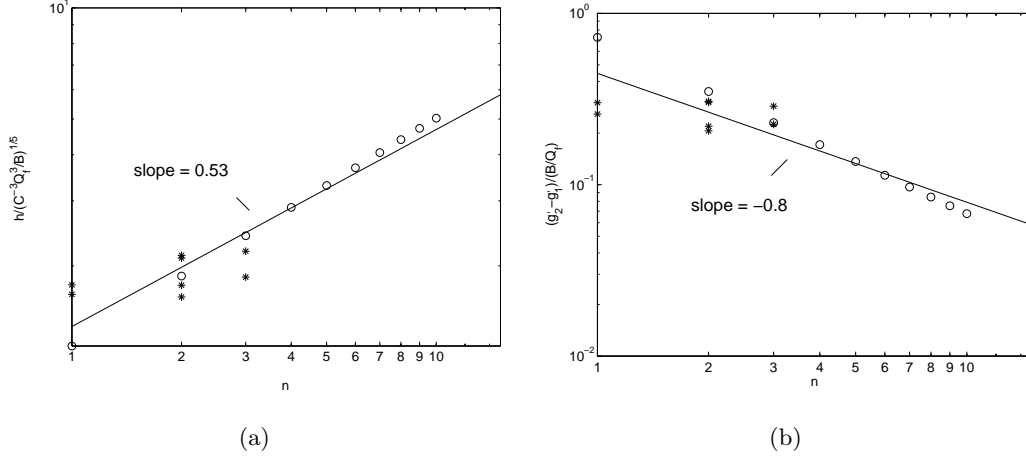


FIGURE 8. (a) The dimensionless interface height  $\frac{h}{(C^{-3}Q_f^3/B)^{1/5}}$  and (b) the non-dimensional density difference  $\frac{g'_2}{B/Q_f} - \frac{g'_1}{B/Q_f}$  plotted against  $n$  with fixed underfloor pressure. The stars are the experimental results and the open circles are the results from the model.

diffusers in case of the same heat load and underfloor pressure. Thus, this analysis shows that the dimensionless stratifications are the same using the dimensionless height and temperature, from (4.1) and (4.2), based on  $Q$ .

The density difference between the two layers can be obtained, using (2.13), (2.14) and (2.15), as

$$\hat{g}_2 - \hat{g}_1 = (g'_2 - \frac{g'_2 Q_e}{Q_e + Q_f}) \frac{Q_f}{B} = \frac{Q_f}{Q_p}. \quad (4.9)$$

Therefore,  $(\hat{g}_2 - \hat{g}_1) \sim \hat{h}^{-\frac{5}{3}} \sim n^{-1}$ .

The experimental results and model predictions are shown in figure 8, where the dimensionless interface height and the dimensionless buoyancy are plotted logarithmically against  $n$ . The best line fits show that  $\hat{h} \sim n^{0.53}$  and  $(\hat{g}_2 - \hat{g}_1) \sim n^{-0.8}$ . These results are consistent with the above scaling analysis.

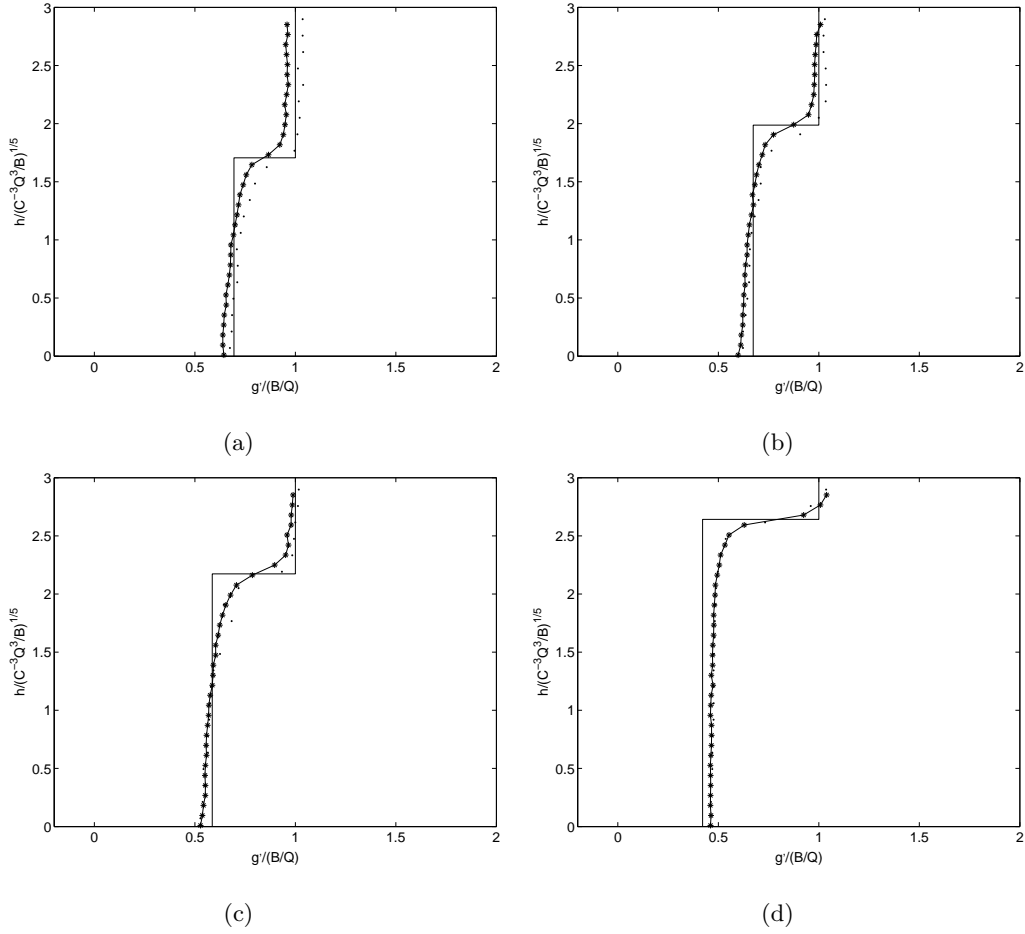


FIGURE 9. Experiment Exp. 3 with its heat source (a) on the floor; (b) at 1/8 of room height; (c) at 1/4 of room height; (d) at 1/2 of room height.

#### 4.2. Effects of an elevated heat source

Figure 9, shows the experimental results from four experiments with identical conditions except for different heights of the heat sources. Here, we use a new dimensionless height  $\hat{z} = z/H$ , since the source height relative to the room height scale  $H$  is a significant parameter. The effect of raising the heat source above the floor is to raise the height of the interface and to decrease the temperature of the lower layer. The upper layer temperature remains constant, since the heat load and the total ventilation rate is the same in each case.

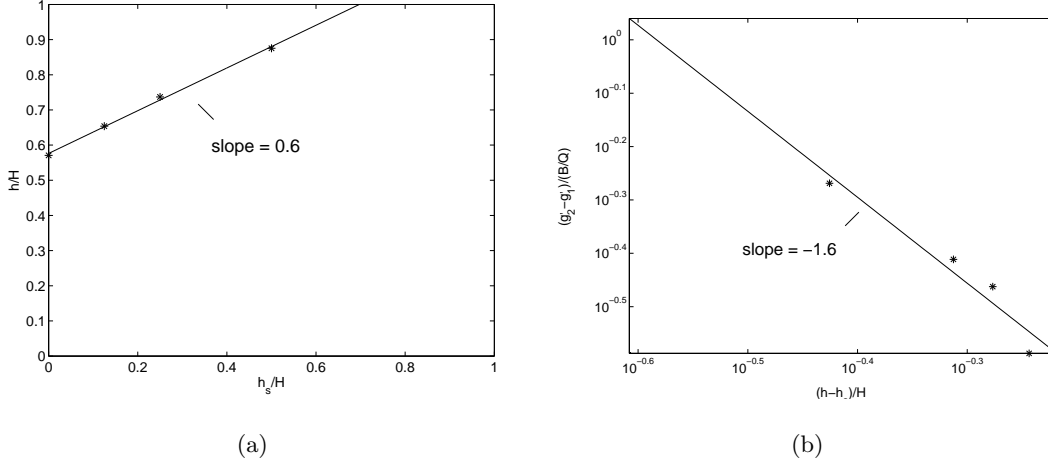


FIGURE 10. (a) The dimensionless interface height  $\frac{h}{H}$  changes with  $\frac{h_s}{H}$  linearly; (b) The dimensionless buoyancy difference between the two layers  $\frac{g'_2}{B/Q} - \frac{g'_1}{B/Q}$  changes with  $\frac{h - h_s}{H}$ .

At interface height  $h$ , the volume flux of an elevated plume is given by

$$Q_p \sim B^{\frac{1}{3}}(h - h_s - z_v)^{\frac{5}{3}}. \quad (4.10)$$

For the parameter range of these experiments the interfacial Richardson number is large enough so that the penetrative entrainment  $E \sim Ri^{-1}$ . Thus,  $Q_e \sim \frac{M^{\frac{3}{2}}}{g' h^2}$ , and (2.16) becomes

$$c_1(h - h_s)^{\frac{5}{3}} = c_2 + \frac{c_3}{h^2}, \quad (4.11)$$

where,  $c_1$ ,  $c_2$  and  $c_3$  are constants. Approximately, (4.11) can be written as

$$\hat{h} - \hat{h}_s \approx c'_2 + \frac{c'_3}{\hat{h}}. \quad (4.12)$$

When  $\hat{h}_s \ll c'_2, c'_3$ , the quadratic (4.12) has roots  $\hat{h} = \frac{1}{2}\hat{h}_s + c''_2$ . Therefore, the effect of an elevated heat source is to produce a linear increase in the interface height, by about one-half the height of the heat source. A least-square fit to the experimental data has a slope of 0.6, as shown in figure 10(a).

Using (4.2), the non-dimensional density difference between two layers  $\hat{g}_2 - \hat{g}_1$  is given as

$$\hat{g}_2 - \hat{g}_1 = \frac{Q_f}{Q_p}, \quad (4.13)$$

so  $(\hat{g}_2 - \hat{g}_1) \sim (\hat{h} - \hat{h}_s)^{-\frac{5}{3}}$ . The experiments in figure 10 show that  $(\hat{g}_2 - \hat{g}_1) \sim (\hat{h} - \hat{h}_s)^{-1.6}$ , which is consistent with this scaling.

## 5. Conclusions

The basic model of a UFAD system consists of a single heat source and a single diffuser. The performance of the whole system depends on entrainment: entrainment into the rising plume above the heat source, entrainment into the negatively-buoyant jet above the diffuser, and finally penetrative entrainment of upper zone temperature into the lower zone as the diffuser flow reverses and falls downwards. Perhaps somewhat surprisingly, provided the diffuser flow has a positive vertical momentum, it always rises high enough to impact the interface, and there is some non-zero penetrative entrainment. Only in the limit of displacement ventilation, where the supply to the lower layer has no vertical momentum, is there zero penetrative entrainment. Then, of course, all the lower zone is at the supply temperature, and the input fluid is neutrally buoyant. Any vertical momentum in this limit will allow the diffuser flow to cross the lower zone until it reaches the warmer upper zone. Thus the controlling feature of the system is the magnitude of the penetrative entrainment  $E$ .

The behavior of UFAD enclosures containing multiple cooling diffusers has been investigated both experimentally and theoretically. A model based on the work of Lin & Linden (2005), in which it is assumed that a two-layer stratification forms, has been extended to predict the room stratification and gives good agreement with the experimental measurements for the layer temperatures and the interface heights.

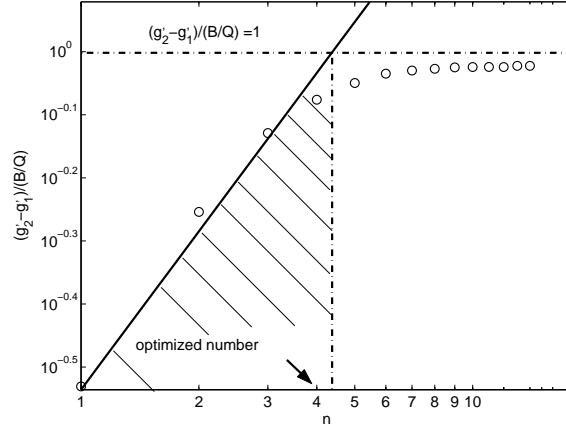


FIGURE 11. A regime diagram showing the region (shaded) where the diffusers work efficiently.

The basic rules that govern the interface height and the temperatures of the two layers as functions of the number of diffusers in multi-diffuser systems, or with the heat source position in elevated-source model, have been determined by scaling analysis and verified by the experiments data. These rules link our extended model to the work of Lin & Linden (2005) quantitatively, and allow the determination of the stratification for any number of diffusers, or for any vertically positioned heat source in elevated-source systems.

In terms of design, these rules are helpful to determine the optimized number of diffusers. Consider, for example, the situation where the total number of diffusers needs to be determined for a space with a given heat load and ventilation flow rate. It may be appropriate that for cost reasons, the number of diffusers should be minimized. The limit of this case is displacement ventilation,  $\hat{g}_2 - \hat{g}_1 = 1$ , when  $n$  is a large. We find the intersection of this point with the scaling law  $\hat{g}_2 - \hat{g}_1 \sim n^{0.9}$ , as shown in figure 11. Thus, the crossing point gives the optimized number  $n = 4$ , of diffusers per heat source, in terms of maximizing the temperature difference and, therefore, the energy savings. For smaller numbers of diffusers, indicated by the shaded region in figure 11, the stratification can be used to make an estimate of the thermal comfort of the space.

The implementation of this model into energy simulation codes requires algorithms

for the temperatures and the interface height, in terms of the input parameters such as the supply temperature, the heat load and ventilation rate. The model described in this paper calculated the diffuser flow by solving the negatively buoyant jet equations numerically. However, it is possible to treat the diffuser flow simply as a jet using similarity theory and this turns out to give a reasonably accurate estimate of the volume flux and, therefore, of the penetrative entrainment rate  $E$ . From a practical viewpoint different diffuser geometries, such as those that induce significant swirl in the flow, can be treated by adjusting the diffuser entrainment constant  $\alpha_f$  (Liu 2005).

This approach of using a simplified model, based on the building blocks of layered stratification and plumes and jets using integral plume equations, provides a rational basis for predicting the performance of UFAD systems. Supported by comparisons with experiments, and comparisons with full-scale data (not reported here), these models allow the performance to be optimized in terms of both energy savings and thermal comfort. This approach also allows other effects, for example the treatment of sources sufficiently close together that their plumes coalesce (Kaye & Linden 2004), to be included in a consistent manner. Other effects, such as using radiant cooling of floors or ceilings can also be included by adding the appropriate heat transfers into the layers. As in the case of natural ventilation these models provide design guidance and a basis for calculating the energy performance of low energy ventilation systems in buildings, based on a rational representation of the physics of the ventilation fluid dynamics.

### **Acknowledgements**

We have worked closely with Fred Bauman and Tom Webster, from the Department of Architecture, at the University of California, Berkeley, in our joint research on UFAD systems. We are grateful for the intellectual companionship they have provided in this



work. We also acknowledge the financial support of the California Energy Commission through Contract 500-01-035 from the PIER buildings program, and the support of Martha Brooks, who has provided leadership in building energy efficiency in California.

#### REFERENCES

- BAINES, W. D. 1975 Entrainment by a plume or jet at a density interface. *J. Fluid Mech.* **68**, 309–320.
- BAINES, W. D. & TURNER, J.S. 1969 Turbulent buoyant convection in a source in a confined region. *J. Fluid Mech.* **37**, 51–80.
- BAUMAN, F. 2004 *Underfloor Air Distribution Design Guide*. The American Society of Heating, Refrigerating and Air-Conditioning Engineers (ASHRAE), University of California, Berkeley.
- BAUMAN, F. & WEBSTER, T. June 2001 Outlook for underfloor air distribution. *ASHRAE Journal* **43 6**, 18–27.
- BLOOMFIELD, L. J. & KERR, R. C. 1998 Turbulent fountains in a stratified fluid. *J. Fluid Mech.* **358**, 336–356.
- BLOOMFIELD, L. J. & KERR, R. C. 2000 A theoretical model of a turbulent fountain. *J. Fluid Mech.* **424**, 197–216.
- BRAGER, G. S., PALIAGA, G & DE DEAR, R. 2004 Operable windows, personal control, and occupant comfort. *ASHRAE Trans.* **110**
- DALZIEL, S. B. 1993 Digimage (image processing software for fluid dynamics). *Tech. Rep.* Department of Applied Mathematics and Theoretical Physics (DAMTP), University of Cambridge, UK.
- FISK W. J. 2000 Health and productivity gains from better indoor environments and their relationship with building energy efficiency. *Ann. Rev. Energy Environ.* **25** 537–566.
- GRAHL, C. L. March 2002 Green Building Quiz: Underfloor Air Distribution Systems. *Environmental Design + Construction*.
- HUNT, G. R. & KAYE, N. G. 2001 Virtual origin correction for lazy turbulent plumes. *J. Fluid Mech.* **435**, 369–377.

- HUNT, G. R. & LINDEN, P. F. 2001 Steady-state flows in an enclosure ventilated by buoyancy forces assisted by wind. *Building and Environment* **36**, 707–720.
- HUNT, G.R., LINDEN, P.F. & COOPER, P. 2001 Thermal stratification produced by jets and plumes in enclosed spaces. *Building and Environment* **36**, 871–882.
- ITO, H. & NAKAHARA, N. 1993 Simplified calculation model of room air temperature profile in under-floor air-condition system. *International Symposium on Room Convection and Ventilation Effectiveness ISRACVE, ASHRAE*.
- KAYE, K.N. & LINDEN, P.F. 2004 Coalescing axisymmetric turbulent plumes. *J. Fluid Mech.* **502**, 41–63.
- KUMAGAI, M. 1984 Turbulent buoyant convection from a source in a confined two-layered region. *J. Fluid Mech.* **147**, 105–131.
- LI, Y. 1993 Role of multizone models in indoor air flow and air quality analysis. *Indoor Environ.* **2**, 149–163.
- LIN, Y.-J. P & LINDEN, P. F. 2005 A model for an under floor air distribution system. *Energy and Building* **37**, 399–409.
- LINDEN, P. F. & COOPER, P. 1996 Multiple sources of buoyancy in a naturally ventilated enclosure. *J. Fluid Mech.* **311**, 177–192.
- LINDEN, P. F., LANE-SERFF, G.F. & SMEED, D.A. 1990 Emptying filling boxes: the fluid mechanics of natural ventilation. *J. Fluid Mech.* **212**, 309–336.
- LINDEN, P. F. 2000 Convection in the environment. *Cambridge Press* UK.
- LINDEN, P. F. 1973 The interaction of a vortex ring with a sharp density interface: a model for turbulent entrainment. *J. Fluid Mech.* **60**, 467–480.
- LIST, E. J. 1982 Turbulent jets and plumes. *Ann. Rev. Fluid Mech.* **14**, 189–212.
- LIU, Q. A. 2005 *The fluid mechanics of underfloor air distribution*. PhD thesis, University of California, San Diego.
- MORTON, B. R. 1959 Forced plumes. *J. Fluid Mech.* **5**, 151–163.
- MORTON, B. R., TAYLOR, G. I. & TURNER, J. S. 1956 Turbulent gravitational convection from maintained and instantaneous sources. *Proceedings of the Royal Society of London A* **234**, 1–23.

- MUSY M., WINKELMAN F. & WURTZ E. 2002 Automatically generated zonal models for building airflow simulation: principles and application. *Building and Environ.* **37**, 873–881.
- REES S. J. & HAVES P. 2001 A nodal model for displacement ventilation and chilled ceiling systems in office spaces. *Building and Environ.* **36**, 753–762.
- ROUSE, H., YIH, C. S. & HUMPHREYS, H. W. 1952 Gravitational convection from a boundary source. *Tellus* **4**, 201–210.
- TURNER, J. S. 1966 Jets and plumes with negative or reversing buoyancy. *J. Fluid Mech.* **26**, 779–792.
- ZHANG, Q. 2001 Room air stratification model for underfloor air distribution system. *MS thesis, University of California, Berkeley.*